

Catalysis Science & Technology

Accepted Manuscript



This is an *Accepted Manuscript*, which has been through the Royal Society of Chemistry peer review process and has been accepted for publication.

Accepted Manuscripts are published online shortly after acceptance, before technical editing, formatting and proof reading. Using this free service, authors can make their results available to the community, in citable form, before we publish the edited article. We will replace this *Accepted Manuscript* with the edited and formatted *Advance Article* as soon as it is available.

You can find more information about *Accepted Manuscripts* in the [Information for Authors](#).

Please note that technical editing may introduce minor changes to the text and/or graphics, which may alter content. The journal's standard [Terms & Conditions](#) and the [Ethical guidelines](#) still apply. In no event shall the Royal Society of Chemistry be held responsible for any errors or omissions in this *Accepted Manuscript* or any consequences arising from the use of any information it contains.

Synthesis factors affecting the catalytic performance and stability of Ru/C catalysts for supercritical water gasification

G. Peng¹, M. Steib^{1†}, F. Gramm³, C. Ludwig^{1,3}, and F. Vogel^{1,4}*

¹General Energy Research Department, Paul Scherrer Institut (PSI), 5232 Villigen PSI, Switzerland

²ENAC-IIE, Ecole Polytechnique Fédérale de Lausanne (EPFL), 1015 Lausanne, Switzerland

³ScopeM, Swiss Federal Institute of Technology Zürich (ETHZ), 8093 Zürich, Switzerland

⁴FHNW, University of Applied Sciences Northwestern Switzerland, 5210 Windisch, Switzerland

* Corresponding author:

E-mail: frederic.vogel@psi.ch.

Tel.: +41 563102135

† Present address: Department of Chemistry, Technical University Munich, 85748 Garching, Germany

Abstract

Catalytic supercritical water gasification of isopropanol (450 °C, 30 MPa) over Ru/C catalysts was carried out in a fixed-bed plug flow reactor. In absence of Ru, isopropanol decomposed to solid carbon (coke), and H₂ over the carbon support. The Ru/C catalyst was able to gasify efficiently 10 wt % isopropanol over a period of 96 h at $WHSV_{gRu} = 1228 \text{ g}_{Org} \text{ g}_{Ru}^{-1} \text{ h}^{-1}$ with the gas composition close to the calculated thermodynamic chemical equilibrium. The catalyst lifetime was affected by the decomposition of isopropanol to solid carbon (coke) over the carbon surface that progressively filled up the pores of the activated carbon and this resulted in a covering of the Ru nanoparticles (NPs). The Ru dispersion (D) was found to be a relevant parameter. The 0.5% Ru/C (D = 0.26) was more active than the 2% Ru/C (D = 0.14). The influence of the solvent (acetone vs. water) used during the catalyst impregnation was studied and the turnover frequency (TOF) was twice higher for the Ru/C catalyst prepared with acetone. The higher Ru dispersion and the lower content of residual chloride obtained for the catalyst prepared with acetone were both responsible.

KEYWORDS: Methane, Carbon, Supercritical water, Isopropanol, Ruthenium

Introduction

Catalytic supercritical water gasification (CSCWG) is a technology under development for converting biomass into gaseous biofuels (such as H₂ and CH₄). In contrast to supercritical water gasification (SCWG) performed at high temperatures (> 600 °C) where close to full conversion of biomass into a H₂-rich product gas can be achieved without catalysts, CSCWG is carried out at low-moderate temperatures (ca. 400 °C). At these conditions, in order to achieve full biomass conversion and a high selectivity towards H₂ or CH₄, a catalyst is needed for decomposing the large organic molecules by C-C bond cleavage¹. For H₂ production, Pt is

reported to have a good catalytic performance in terms of activity and selectivity for CSCWG of methanol, ethanol, and ethylene glycol². An optimal catalyst for enhancing H₂ formation should have a high activity for C-C bond cleavage, favor the water gas shift reaction ($\text{CO} + \text{H}_2\text{O} \rightarrow \text{H}_2 + \text{CO}_2$) for an increased H₂ yield, as well as minimize the methanation reaction ($\text{CO}_x + (2+x) \text{H}_2 \rightarrow \text{CH}_4 + x \text{H}_2\text{O}$). In contrast, for CH₄ production, the catalyst should enhance the methanation reaction, besides C-C bond cleavage and water gas shift activity. Ru has been found to be the most active and selective metal towards CH₄ formation by facilitating also the C-O bond cleavage³. Previous work⁴ has already shown the good catalytic performance of a commercial Ru/C catalyst for CSCWG of synthetic liquefied wood (SLW) over a period of 220 h as well as its high CH₄ selectivity. Most of the CSCWG studies⁴⁻²² performed in continuous mode have been carried out with water-soluble model compounds such as glycerol, sorbitol, ethylene glycol, cresol, phenol, and glucose. Among these water-soluble compounds organic acids and alcohols have a greater relevance due to their presence as intermediate products during SCWG of real biomass and their relatively good stability in supercritical water (SCW)²³. Carboxylic acid compounds are potentially more problematic to gasify than alcohols because they may form coke precursors decreasing the catalyst lifetime. De Vlieger et al.² observed that reforming of acetic acid over Pt/Al₂O₃ catalysts at 275 °C and 25 MPa led to a fast catalyst deactivation within 3 h due to coke deposition on the catalyst surface while no deactivation was observed when reforming other alcohols (methanol, ethanol) during 5 h of CSCWG. Dreher et al.²⁴ have also reported the decrease of the catalyst lifetime after 3 h on-stream when gasifying 21 wt % acetic acid over a 2% Ru/C catalyst at 390 °C and 25 MPa. It was suggested that the polymerization rate of acetic acid dominated the overall gasification rate at subcritical conditions leading to coke deposition on the catalyst. Recently, De Vlieger et al.²⁵ found out that a carbon nanotube (CNT) supported Ru catalyst was stable during reforming of acetic acid at 270 °C and 23 MPa and also at 400 °C and 25 MPa, while in the subcritical region (340 °C, 23 MPa) a fast deactivation was observed. The

high ionic product (K_w) at subcritical conditions was the cause for the catalytic deactivation observed. In this work, for minimizing any fast catalyst deactivation caused by coke deposits, isopropanol as a model compound is used. Due to the harsh conditions of SCW, only a few catalyst supports were reported to be stable like rutile-TiO₂, α -Al₂O₃, ZrO₂ and carbon^{5,26}. Here, the motivation for using carbon is mainly due to its higher specific surface area ($> 500 \text{ m}^2 \text{ g}^{-1}$) compared to metal oxides ($< 150 \text{ m}^2 \text{ g}^{-1}$) allowing for a higher Ru dispersion. In addition, carbon has other advantages like a high resistance to acidic and basic media, a good stability at high temperature and in aqueous media, the possibility to modify its chemical surface properties by adding anchoring groups, the recovering of the active phase of the used catalyst after reaction by combustion (crucial if the active phase is a noble metal), and a low price. The severe conditions of SCW imply the use of a stable Ru/C catalyst having a high activity and selectivity towards CH₄. We studied first the stability of the physical structure of the carbon support in SCW conditions in order to assess its potential to be used as a catalyst support. Secondly, we studied the catalytic performances of the Ru/C catalysts by operating at low and high weight hourly space velocity. The Ru dispersion effect was assessed by preparing two catalysts with different Ru loadings, i.e. 0.5 wt % and 2 wt % Ru, respectively. Finally, the effect of the solvent (water vs. acetone) used during catalyst impregnation was also investigated.

Experimental section

Catalyst preparation and characterization

A granular carbon material (denoted here as Org10_CO from Desotec) was sieved to a size fraction of 0.3-0.8 mm. The carbon support was impregnated with RuCl₃·xH₂O as the salt precursor (99.9%, Alfa Aesar) in a water (Ru/C_w) or in an acetone (Ru/C_a) solution for 24 h, followed by solvent evaporation in a rotary evaporator and washed with pure water during filtration. ICP-OES (Liberty 110, Varian) measurements of the filtrate were undertaken to

detect any Ru loss during washing. After drying in an oven at 90 °C overnight, the catalyst was reduced under flowing H₂ (20 mL min⁻¹) at 450 °C during 4 h for chloride removal. Two different Ru loadings were prepared: 0.5 and 2 wt % Ru from a water or acetone solution containing the dissolved ruthenium precursor. The Ru loading was determined by measuring the dissolved Ru concentration in the solution before and after impregnation by ICP-OES, taking into account Ru losses during catalyst washing. The catalysts were characterized by H₂-temperature-programmed reduction (H₂-TPR) and CO pulse chemisorption in a fully automated instrument (TPD/R/O 1100, Thermo Scientific) connected to a TCD and to a mass spectrometer (GAM 400). For each H₂-TPR measurement, 0.1 g of sample was weighted and heated (10 °C min⁻¹) from room temperature (RT) to 350 °C under flowing Ar (20 mL min⁻¹) and then kept at this temperature for 30 min to remove impurities and water. Then the sample was cooled to RT and passivated with O₂/He (5:95, 20 mL min⁻¹) at 100 °C for 30 min. Finally, the sample was cooled to RT again and the gas was switched to H₂/Ar (10:90, 20 mL min⁻¹). TPR was performed from RT to 450 °C with a temperature ramp of 10 °C min⁻¹. For the CO pulse chemisorption, the sample was reduced under H₂/Ar (10:90, 20 mL min⁻¹) at 450 °C for 4 h in order to clean the ruthenium surface from any deposited carbon species. Then it was flushed with pure He at 450 °C for 1.5 h to remove H₂ from the catalyst and finally cooled down to RT. The CO pulses were carried out with CO/He (20:80) at RT. The dispersion was calculated by assuming 1 as the stoichiometric factor for CO:Ru. The following formula was used for determining the Ru dispersion:

$$D_{\text{CO}} = \frac{N_{\text{ads}} \cdot F_s \cdot 10 \cdot M_{\text{met}}}{X_{\text{met}}} \quad (1)$$

where N_{ads} is the amount of gas adsorbed during pulse chemisorption (mmol g⁻¹); F_s corresponds to the stoichiometric factor (moles of metal/moles of gas); M_{met} is the metal atomic weight (g mol⁻¹) and X_{met} is the metal loading on a mass basis (wt %). The average metal particle sizes were calculated as:

$$d_{p,CO} = \frac{d_{at} \cdot 5.01}{D_{CO}} \quad \text{for } D_{CO} < 0.2 \quad (2)$$

where d_{at} is the atomic diameter of Ru ($d_{at} = 2.6 \text{ \AA}$)²⁷. N₂-physisorption measurements were performed with an Autosorb-1 (Quantachrome Instruments) for determining the porosity and the BET specific surface area (BET SSA). The total pore volume was measured at $p/p_0 = 0.99$ and the mesopore volume with the t-plot method. Prior to N₂-physisorption degassing under He at 300 °C for 6 h was carried out for all the samples. The Ru NPs were characterized by Scanning Transmission Electron Microscopy (STEM). The measurements were performed with an aberration corrected dedicated STEM microscope (Hitachi HD-2700 CS), operated at an acceleration voltage of 200 kV and equipped with a high angle annular dark field (HAADF) detector. For each sample, different areas were carefully selected in order to have a reliable representation of the average Ru NPs size. The average Ru NPs size and the dispersion (D_{STEM}) were calculated as:

$$d_{p,STEM} = \frac{\sum_i n_i d_i^3}{\sum_i n_i d_i^2} \quad (3)$$

$$D_{STEM} = 1.23 \sqrt{\frac{d_{at} \cdot 3.32}{d_{p,STEM}}} \quad \text{for } 0.2 \leq D_{STEM} \leq 0.92 \quad (4)$$

where n_i is the number of particles with diameter d_i ²⁷. Thermogravimetric analysis (TGA) was conducted in a thermogravimetric analyzer (TGA; NETZSCH STA 449 C). A 0.01 g of sample was loaded and heated from RT to 110 °C under Ar atmosphere for 30 min and then heated up to 900 °C at 10 °C min⁻¹ under flowing O₂/Ar (10:90, 10 mL min⁻¹). CNS elemental analysis was performed with an elemental analyzer (Vario EL cube, Elementar). X-ray Photoelectron Spectroscopy (XPS) was carried out with a VG Escalab 220i XL apparatus by using a monochromatic Al K α ($h\nu = 1486.6 \text{ eV}$) radiation as the X-ray source.

Experimental setup

The physical structure stability of the carbon support in SCW conditions was assessed with an unstirred stainless steel mini-batch reactor (HIP, 316 SS) having a volume of 5 mL. A 0.5 g of the carbon support was added with 1.5 g of water into the reactor. Then, it was tightly closed and placed into a fluidized sand bath (Techne SBL-2D) to be heated up to 420 °C under 35 MPa for 5 h. After cooling, the carbon support was recovered by filtration and dried at 110 °C overnight. A second run of 5 h following the same procedure was undertaken in order to reach 10 h of SCW treatment. CSCWG experiments of isopropanol were carried out in a fixed-bed plug flow (PF) reactor (see Figure 1). The feed (F-1) and the water (F-2) were pumped by an HPLC pump (Waters 515) at a constant mass flow rate ($F = 3$ g/min). For accurate mass flow rate measurements, the feed tank was put on an analytical balance (Mettler Toledo PG6002-S). A manual valve (V-1) allowed switching from the water to the feed effluent. A preheater was needed for assuring isothermal conditions along the catalyst bed. The PF reactor consisted of a stainless steel tube (SITEC) with a length of 40 cm, internal diameter of 0.8 cm (total $V_{\text{reactor}} = 20$ mL). The catalyst loading was around 0.15-0.6 g depending on the experiment. The first 35 cm of the reactor were filled with a carbon material ($0.8 < \text{diameter} < 2$ mm). A movable thermocouple (T1) was installed within the reactor for recording temperature during CSCWG. The PF reactor was placed in an electric oven for heating. The reactor effluent passed through a metal filter (2 μm) to retain any solid particles. The fluid was cooled down by passing through a water tank. A safety valve (V-2) was installed for preventing any overpressure in the system. The pressure in the system was maintained by a backpressure regulator (V-3). Finally, the gas and the liquid were separated at ambient conditions in a phase separator made of glass. The gas was collected in a sample bag (3L SKC) at different time intervals and analyzed by gas chromatography. The liquid samples were stored in 40 mL flasks and analyzed off-line with a TOC analyzer. The temperature (T1) and the pressure (P1) were recorded continuously with a computer using LabView.

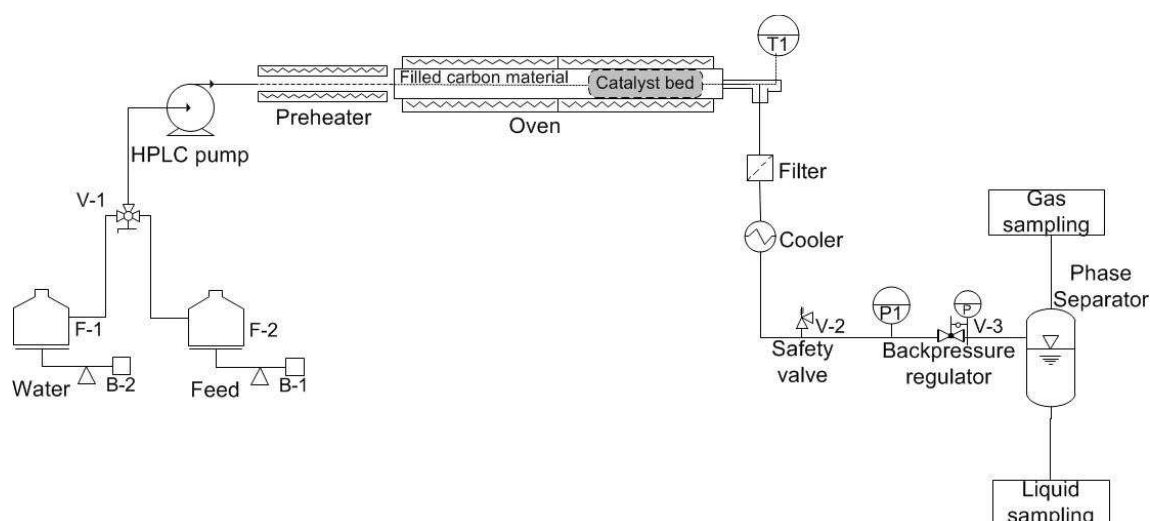


Figure 1. Schematic of the fixed-bed plug flow reactor setup for continuous CSCWG.

Analytical methods for the gaseous and liquid effluents

The gas phase was analyzed off-line with a gas chromatograph (HP 6890, columns: HP-Plot Q 30m x 0.53mm x 40 μ m and HP-Plot Molecular Sieve 5A, 30m x 0.53mm x 40 μ m) with helium as the carrier gas using a Thermal Conductivity Detector (TCD) to detect CO₂, CH₄, CO, and H₂ and a Flame Ionization Detector (FID) for higher hydrocarbons (C₂H₆ and C₃H_x). The liquid samples were collected manually at regular intervals, and their total organic carbon (TOC) content was measured with a TOC analyzer (Elementar). The liquid samples were also analyzed by GC-MS (Agilent 5975C).

Chemical equilibrium composition

The thermodynamic chemical equilibrium calculation was performed using the Aspen Plus® simulation package by using the Peng-Robinson equation of state. The values for the gas composition at the thermodynamic chemical equilibrium (450 °C, 30 MPa and 10 wt % isopropanol) are: CO₂ = 24.7 vol %; CH₄ = 65.6 vol %; H₂ = 8.7 vol %; CO = 0.7 vol %.

Terms and definitions

For comparing the catalytic performances based on the Ru amount, the weight hourly space velocity normalized to one gram of Ru (WHSV_{gRu}) is used:

$$\text{WHSV}_{\text{gRu}} = \frac{\dot{m}_{\text{Org}}}{W_{\text{Ru}} \cdot \text{time}} \quad (5)$$

The observed activity is defined as the total organic carbon conversion (X_c) from the feed to the liquid effluent:

$$X_c (\%) = 1 - \frac{\text{TOC}_{\text{Out}}}{\text{TOC}_{\text{Feed}}} \cdot 100\% \quad (6)$$

The carbon gasification efficiency (GE_c) is the relation between the total amount of carbon in the gas phase and the total amount of carbon in the feed, defined as:

$$\text{GE}_c (\%) = \frac{\text{Total mol C}_{\text{Gas}}}{\text{Total mol C}_{\text{Feed}}} \cdot 100\% \quad (7)$$

The rate of coke deposition ($R_{\text{Coke dep.}}$) is calculated from a carbon mass balance as follows:

$$R_{\text{Coke dep.}} \left(\text{mmol C min}^{-1} \right) = \dot{n}_{\text{C,Feed}} - \dot{n}_{\text{C,Reactor effluent}} - \dot{n}_{\text{C,Gas}} \quad (8)$$

The observed turnover frequency (TOF) was calculated as the total mole of isopropanol consumed per active Ru site (measured by STEM) per second:

$$\text{TOF}(\text{s}^{-1}) = \frac{-\Delta \text{mol}_{\text{isop.}}}{\text{mol}_{\text{Ru}} \cdot D_{\text{STEM}} \cdot \text{time}} \quad (9)$$

Results and discussion

Physical structure stability of the carbon support in SCW

Prior to active phase impregnation, it is necessary to ensure the good physical structure stability of the carbon support in order to prevent any activity loss due to a structure collapsing. To this aim its physical structure stability was tested at SCW conditions in a mini-batch reactor at 420 °C and 35 MPa for 5 and 10 h. As shown in Table 1, the physical structure of the carbon support after 5 and 10 h in SCW conditions was relatively well preserved. Some slight modifications of the meso/micropore volume can be observed suggesting that the SCW caused more micropores and less mesopores. The increase of the micropore volume in SCW was likely due to the removal of some impurities trapped in the micropores. We can also appreciate the high specific surface area ($> 700 \text{ m}^2 \text{ g}^{-1}$) of this material. In comparison with refractory metal oxides like $\alpha\text{-Al}_2\text{O}_3$, *rutile*- TiO_2 or ZrO_2 , which were reported^{26,28–30} to be stable in SCW conditions, their specific surface area is much lower and does not exceed $150 \text{ m}^2 \text{ g}^{-1}$. Thus, the potential for achieving highly dispersed Ru NPs on the carbon support appears to be much higher.

Table 1. Physical structure evolution of the carbon support at SCW conditions (420 °C, 35 MPa).

Sample	BET SSA [$\text{m}^2 \text{ g}^{-1}$]	$V_{\text{mesop.}}$ [$\text{cm}^3 \text{ g}^{-1}$]	$V_{\text{microp.}}$ [$\text{cm}^3 \text{ g}^{-1}$]
Fresh C	802	0.69	0.14
After 5 h in SCW	779	0.56	0.18
After 10 h in SCW	717	0.45	0.17

Catalyst characterization results

The characteristics of the Ru/C catalysts are presented in Table 2.

Table 2. Characteristics of the fresh Ru/C catalysts.

Sample	BET SSA	V _{mesop.}	V _{microp.}	Ru loading	H ₂ consumption ^a	D _{CO}	D _{STEM}	d _{p,CO}	d _{p,STEM}
	[m ² g ⁻¹]	[cm ³ g ⁻¹]	[cm ³ g ⁻¹]	[wt %]	[μmol/g]	[-] ^b	[-] ^c	[nm] ^b	[nm] ^c
Fresh C	802	0.69	0.14	0	0	N.A.	N.A.	N.A.	N.A.
0.5% Ru/C _w	765	0.75	0.13	0.6	3.5	0.12	0.26	11	5 ± 1.2
2% Ru/C _w	737	0.73	0.11	2.3	32.0	0.08	0.14	16	10 ± 2.7
2% Ru/C _a	619	0.54	0.11	2.1	46.6	0.11	0.35	12	3 ± 0.6

^a Determined from H₂-TPR.

^b Determined by CO pulse chemisorption.

^c Determined by STEM.

The specific surface area was affected by the impregnation with Ru and was found to decrease with the Ru loading for the Ru/C_w catalysts. A higher Ru loading led to a larger Ru NP size, which reduced the pore volume and the specific surface area. The Ru NPs cannot be located inside the micropores because the micropores are too small (< 2 nm) for the Ru NPs. The fact that the micropore volume decreases slightly after impregnation could be due to the blockage of the entrance of some of the micropores. The decrease of the mesopore volume of the 2% Ru/C_a suggests that some Ru NPs are located in the mesopores. Whereas the conservation of the mesopore volume of the 0.5% Ru/C_w and 2% Ru/C_w indicates that the Ru NPs are rather in the macropores. In Figure 2, the Ru NPs for the 0.5% Ru/C_w, 2% Ru/C_w, and 2% Ru/C_a catalysts are shown, the white dots correspond to the Ru NPs. According to the CO pulse chemisorption and the STEM measurements, the use of acetone is more favorable for achieving a better Ru dispersion. By looking at the histograms of the particle sizes, the

Ru/C catalysts prepared with water exhibit a much broader Ru NPs size distribution proving thus the advantage of using acetone during the catalyst preparation in order to obtain a narrow distribution. As mentioned elsewhere³¹ acetone is able to favor a higher interaction between RuCl₃ and the hydrophobic surface of carbon during the impregnation leading to a higher Ru dispersion.

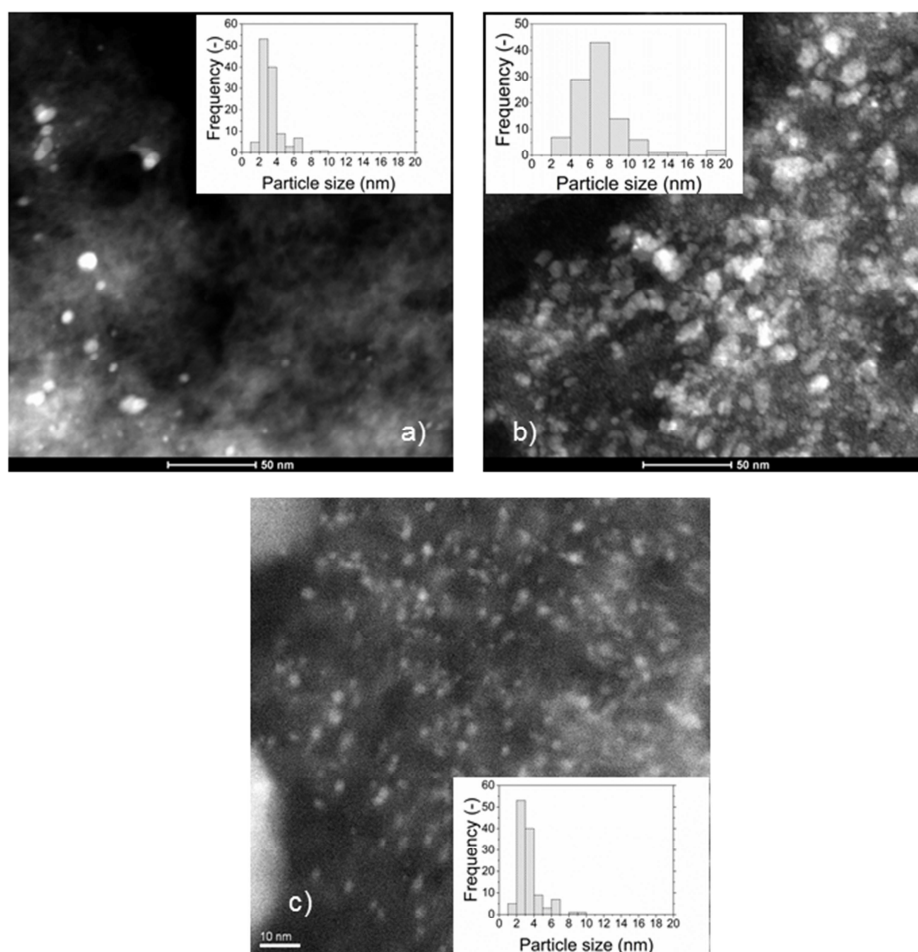


Figure 2. HAADF-STEM images of the (a) 0.5% Ru/C_w, (b) 2% Ru/C_w, and (c) 2% Ru/C_a catalysts.

Interestingly, the Ru NPs size values obtained by CO pulse chemisorption have been overestimated (by 6-9 nm) for all the catalysts. As an explanation the presence of residual chloride coming from the salt precursor (RuCl₃) may be the cause. It is also known^{32,33} that residual chloride reduces the CO adsorption capacity of the catalyst by poisoning the surface of the Ru NPs. As illustrated in Figure 3, some residual chloride species were detected on the

2% Ru/C_w (0.28 at%) by XPS, while no chloride species were found on the 2% Ru/C_a. Yin et al.³¹ have also observed that the Ru/C catalysts prepared with acetone resulted in a lower concentration of residual chloride in comparison to the catalysts prepared by water. According to them, water enhances the anchoring of residual chloride on the carbon support during the catalyst preparation.

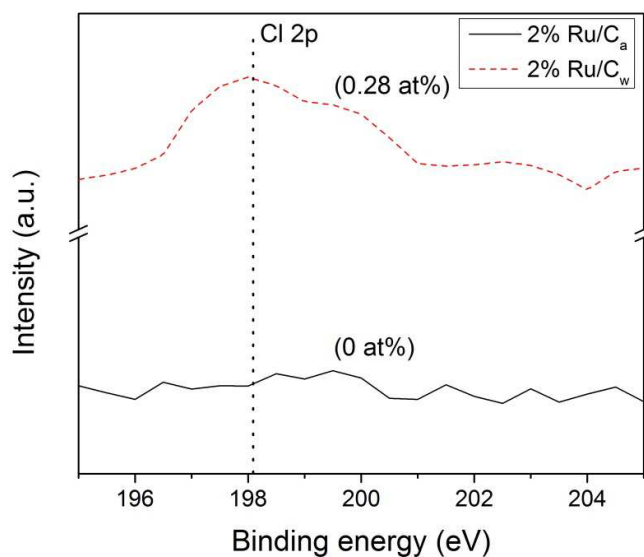


Figure 3. Cl 2p (198.1 eV) XPS patterns of 2% Ru/C_w and 2% Ru/C_a catalysts.

In Figure 4, the H₂-TPR results show a first reduction peak at ca. 100-110 °C corresponding to the reduction of RuO₂ to Ru⁰ as reported by Rossetti et al.³⁴. The reduction peak for the catalysts prepared with water is slightly lower (104 °C) than for the one prepared with acetone (111 °C). Yin et al.³¹ have also observed this shift to higher temperature when using acetone. According to them, the use of acetone renders the reduction of the precursor more difficult. Their explanation is a higher interaction between RuO₂ and the carbon support. The lower H₂ consumption for the 2% Ru/C_w in comparison to the 2% Ru/C_a was likely due to the higher Ru dispersion for the catalyst prepared with acetone. On the other hand, the presence of residual chloride on the Ru/C_w catalysts can also explain the lower H₂ consumption as

mentioned by Guerrero-Ruiz and al.³⁵. About the other peaks around 240 °C, 260 °C, 330 °C, and 440 °C, MS analysis has identified CH₄ formation suggesting hydrogenation of carbon oxides (surface functional groups) to CH₄ or of other weakly bonded carbon species³⁵. The reduction of these carbon oxides/surface species is supposed to occur in the vicinity of the Ru NPs because both the hydrogen dissociation and the hydrogenation are catalyzed by Ru. These additional reduction peaks are absent for the 0.5% Ru/C_w due to the low amount of Ru.

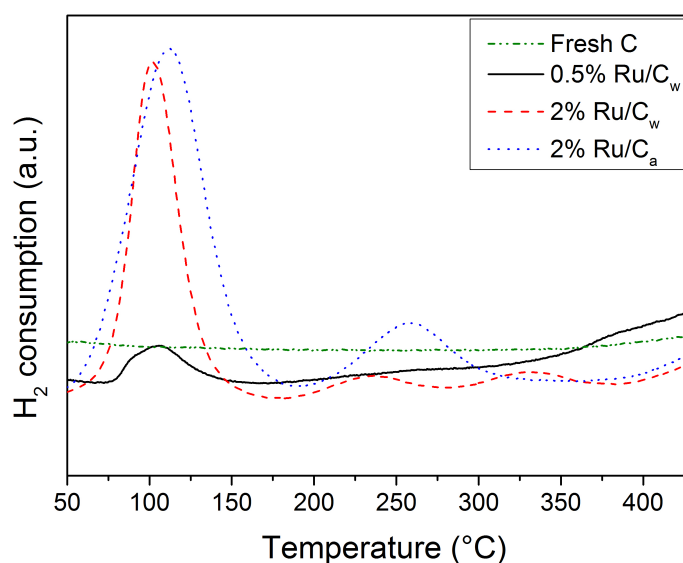


Figure 4. H₂-TPR profiles of the fresh C, 0.5% Ru/C_w, 2% Ru/C_w, and 2% Ru/C_a catalysts.

Blank SCWG experiment

The first SCWG experiment aimed at assessing the stability of isopropanol under SCW conditions in the absence of a catalyst as well as at checking the catalytic activity of the reactor wall. A blank experiment with an empty reactor was carried out at 450 °C and 30 MPa and a residence time of 59 s (density of water at reaction conditions is 148 g L⁻¹). The total organic carbon conversion (X_C) was close to zero, and no gas production was measured indicating the inertness of the reactor wall as well as the stability of isopropanol at these

conditions. GC-MS analysis confirmed that isopropanol was stable since no decomposition products were found. For the next experiment, the reactor was filled only with the support carbon material in order to check its activity during SCWG. According to Figure 5, X_C decreased steadily from 82% to 12% during the first 6 h of gasification. Such a high initial activity of the carbon support was not expected. In Table 3, the results of the SCWG after 24 h are summarized.

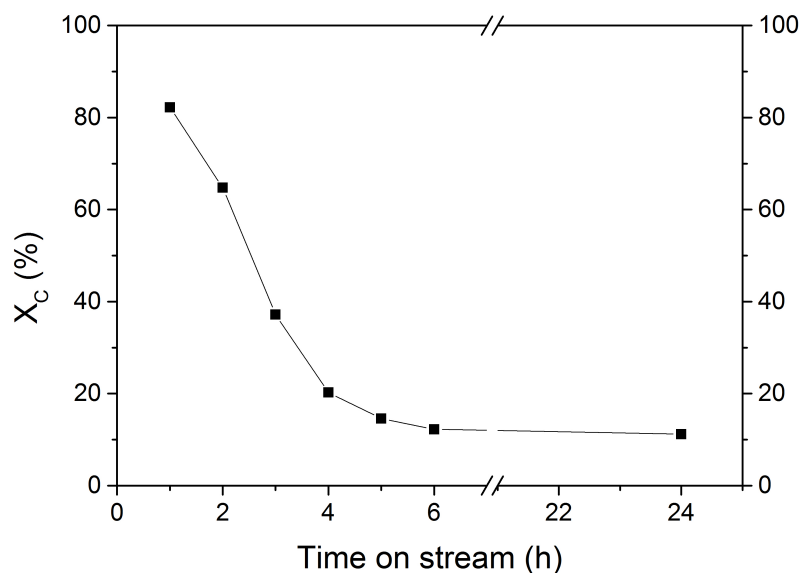


Figure 5. SCWG of 10 wt % isopropanol over the carbon support material at 450 °C and 30 MPa during 24 h on-stream with $F = 3 \text{ g min}^{-1}$.

Table 3. Results of the SCWG of 10 wt % isopropanol over the neat carbon support material performed at 450 °C and 30 MPa during 24 h with $F = 3 \text{ g min}^{-1}$.

Sample	Time [h]	X_c [%]	GE_c [%]	$R_{\text{Coke dep.}}$ [mmol C min ⁻¹]	Gas composition [vol %]					
					CH ₄	CO ₂	H ₂	CO	C ₂ H ₆	C ₃ H _x
Fresh C	24	11	4	1.2	3.3	0.5	96	0.2	< 0.1	5

The absence of high concentrations of CO (and CO₂) indicates that the C-O bond in isopropanol is efficiently broken. The low methane concentration shows that the methanation reaction is not favored in the absence of the catalyst, and the presence of C₃H_x indicates that isopropanol lost its hydroxyl group by reacting with the carbon surface. Interestingly, the carbon gasification efficiency (GE_C) was much lower than X_C, meaning that the carbon contained in the feed was only partially converted to the gas phase. Based on the GE_C and X_C values after 24 h on-stream, a carbon accumulation of ca. 1.2 mmol C min⁻¹ has been calculated. Thus a plausible explanation of the observed trend in activity is that the isopropanol decomposed to H₂, water, and solid carbon (coke) on the surface of the carbon support, whose pores were progressively filled up by the coke, thereby reducing the activity of the support. Unlike carboxylic acid compounds which tend to polymerize before reaching the active phase leading to catalyst deactivation²⁴, it seems that isopropanol underwent decomposition on the catalyst support itself. The liquid effluent was analyzed by GC-MS and the result showed that isopropanol was the main product in the liquid phase. However, the presence of a small amount of benzene was recorded. Chakinala et al.²³ have studied the conversion of 1-propanol at SCW conditions (600 °C, 25 MPa) in a batch reactor for 15 min and also observed the formation of a small quantity of benzene, confirming the occurrence of aromatization reactions. In summary the carbon surface was active enough for decomposing isopropanol to coke and H₂, likely due to impurities and/or surface functional groups.

In Table 4, it can be seen that the absence of Ru led to a complete loss of the microporosity as well as a considerable loss of the mesoporosity after 24 h. These results are relevant because they show that if isopropanol cannot be entirely converted to gaseous products, it reacts with the carbon surface to form coke resulting in a drastic loss of the porosity. The fact that also the mesopores are affected by coke formation means that the coke is likely to deposit also on the Ru NPs, which would lead to the deactivation of the catalyst.

Table 4. Physical structure evolution of the carbon support after 24 h of SCWG with 10 wt % isopropanol (450 °C, 30 MPa).

Sample	BET SSA [m ² g ⁻¹]	V _{mesop.} [cm ³ g ⁻¹]	V _{microp.} [cm ³ g ⁻¹]
Fresh C	802	0.69	0.14
C after SCWG	84	0.21	0

A TGA study was carried out in order to confirm the presence of coke deposits after SCWG with isopropanol. As shown in Figure 6, the carbon support after SCWG of isopropanol started to oxidize at a lower temperature (400 °C) than the fresh carbon support (500 °C). These results, although not very conclusive, support the presence of less thermally stable carbon species (i.e. coke deposits) on the used carbon support after SCWG of isopropanol. The carbon support appears to be more thermally resistant after the SCWG treatment since the maximum consumption peak was shifted from 620 °C to 645 °C. The removal of –CH₂ and –CH groups during the SCWG treatment might be the reason for the enhancement of the thermal resistance of the support³⁶. A diminution of the amount of ash was also observed in the TGA. At 900 °C, the weight loss of the fresh carbon support remained constant at 9 mg meaning that 1 mg of ash remained, whereas for the used carbon the remaining ash was only 0.2 mg.

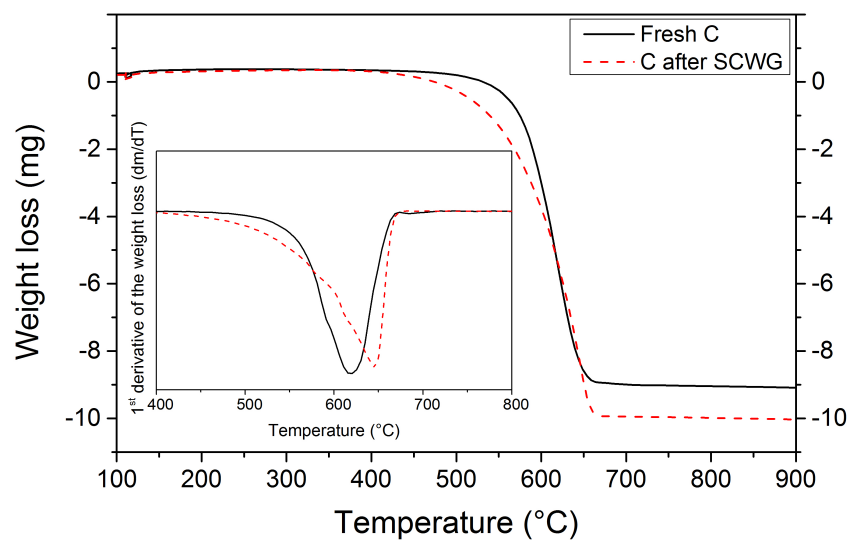


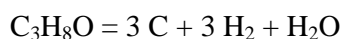
Figure 6. TGA and DTA study of the fresh carbon support and of the carbon support after SCWG with 10 wt % isopropanol (450 °C, 30 MPa). Initial sample mass was 10 mg for both samples.

Finally, as shown in Table 5, the CNS elemental analysis of the carbon support confirmed the presence of additional carbon after SCWG, while nitrogen and sulfur concentration remained both constant.

Table 5. CNS elemental analysis of the fresh carbon support and of the carbon support after SCWG with 10 wt % isopropanol (450 °C, 30 MPa).

Sample	C [wt %]	N [wt %]	S [wt %]
Fresh C	68 ± 2	0.41 ± 0.01	0.24 ± 0.02
C after SCWG	85 ± 1	0.43 ± 0.02	0.26 ± 0.04

To explain these results we propose a decomposition of isopropanol on the surface of the support to form elemental carbon (“coke”), H₂, and water according to:



Thus, the average carbon content of the support after SCWG of isopropanol would increase, as shown in Table 5. The measured gas composition, i.e. 96 vol % H₂, further supports this hypothesis (see Table 3).

CSCWG over Ru/C catalysts

The CSCWG experiments aim at assessing the catalytic performance of the Ru/C catalysts. In Figure 7, CSCWG of 10 wt % isopropanol over the 2% Ru/C_a catalyst is presented. During the first hours on-stream the liquid effluent was collected in order to detect any leaching of Ru. The analysis of the effluent by ICP-OES did not reveal any Ru showing the strong interaction between the carbon support and Ru. At a relatively low weight hourly space velocity (1228 g_{Org} g_{Ru}⁻¹ h⁻¹), the observed total carbon conversion was 99% during the first 28 h and began slowly to decrease to 90% after 96 h of CSCWG. However, as illustrated in Table 6, even at X_C = 90% the gas composition was close to the thermodynamic chemical equilibrium. GE_C was similar to X_C proving that all the carbon contained in the feed was fully converted to the gas phase with no noticeable coke deposition within the reactor (R_{Coke dep.} ≈ 0). Nevertheless, it is worth noting that GE_C values are less accurate than X_C values obtained by TOC analysis. The main reasons are that gas flow rate measurements are not always accurate due to some gas accumulation inside the setup, and fluctuations of the mass flow rate. As a consequence, the observed activity is calculated solely from X_C in this work.

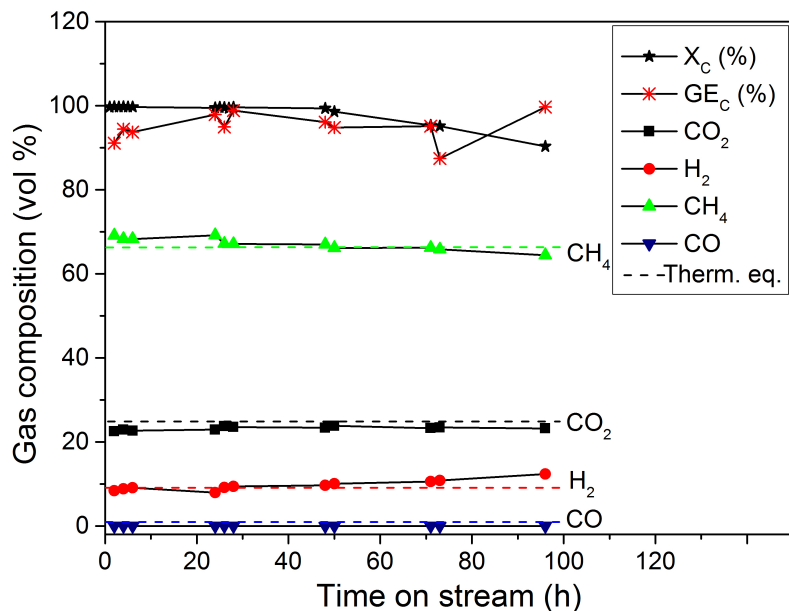


Figure 7. CSCWG of 10 wt % isopropanol over the 2% Ru/C_a catalyst at 450 °C and 30 MPa for 96 h on-stream with $\text{WHSV}_{\text{gRu}} = 1228 \text{ g}_{\text{Org}} \text{ g}_{\text{Ru}}^{-1} \text{ h}^{-1}$. The dashed lines denote the calculated thermodynamic equilibrium concentrations.

Table 6. Results summary after 96 h of CSCWG with 10 wt % isopropanol over the 2% Ru/C_a catalyst at 450 °C and 30 MPa with $\text{WHSV}_{\text{gRu}} = 1228 \text{ g}_{\text{Org}} \text{ g}_{\text{Ru}}^{-1} \text{ h}^{-1}$.

Catalyst	Time [h]	X_c [%]	GE_c [%]	$R_{\text{Coke dep.}}$ [mmol C min ⁻¹]	Gas composition [vol %]					
					CH ₄	CO ₂	H ₂	CO	C ₂ H ₆	C ₃ H _x
2% Ru/C _a	96	90	100	≈ 0	64.4	23.2	12.4	< 0.1	< 0.1	< 0.1

It is well known that most of the catalytic reactions occur at the surface of the active phase, often meaning that higher metal dispersion results in better activity. Hence, it is essential to assess the Ru dispersion effect on the catalytic performance. As illustrated in Figure 8 and in Table 7, a relevant effect of the Ru dispersion was observed where the 0.5% Ru/C_w exhibited a higher activity, i.e. a higher carbon conversion X_c , than the 2% Ru/C_w after 6 h of CSCWG

when basing the WSHV on the amount of Ru, not on total catalyst mass. Interestingly, the TOF for the 0.5% Ru/C_w and 2% Ru/C_w were almost equal. In a recent study, Masini et al.³⁷ have reported that larger Ru NPs (7-10 nm) were a bit more active than smaller NPs (4 nm) for the methanation reaction carried out in gas-phase confirming the structure sensitivity of the methanation. The presence of a higher concentration of under-coordinated sites (e.g. kinks or steps) on the larger Ru NPs was responsible for the catalytic activity enhancement. In fact, Vendelbo et al.³⁸ demonstrated that the CO bond dissociation only occurs on the steps of Ru. The high capability for the CO bond dissociation is crucial since the latter is reported to be the rate-determining step for the methanation reaction^{38,39}. Due to the broad particle size distribution of the Ru/C_w catalysts (see Figure 2) it is impossible to assess the Ru NPs effect and thus to conclude the structure sensitivity of the methanation reaction from our data.

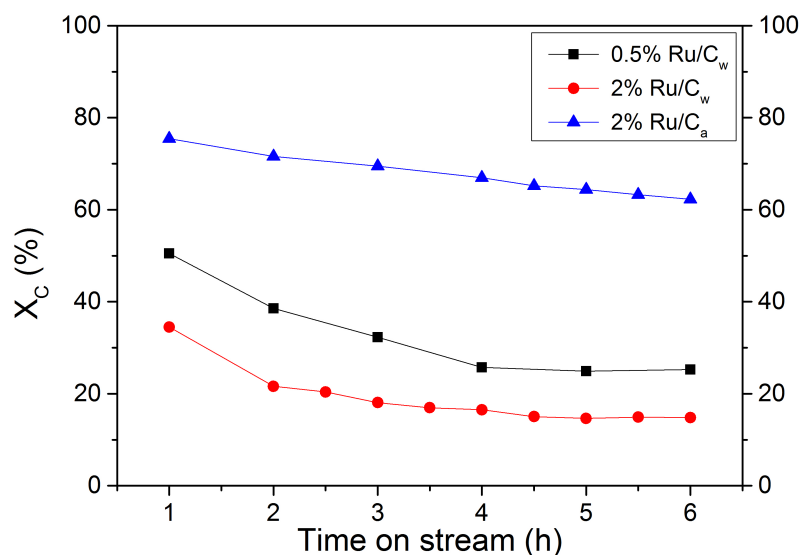


Figure 8. Assessment of the Ru dispersion effect and the solvent effect during CSCWG of 10 wt % isopropanol at 450 °C and 30 MPa with $\text{WHSV}_{\text{gRu}} = 5202 \text{ g}_{\text{Org}} \text{ g}_{\text{Ru}}^{-1} \text{ h}^{-1}$.

A relevant effect of the solvent used during catalyst preparation was found where the activity after 6 h for the 2% Ru/C_a was higher than the 2% Ru/C_w. As it can be seen in Table 7, the TOF was found to be twice smaller for the 2% Ru/C_w. Such a high difference cannot

only be explained by the higher Ru dispersion but mainly by the lower concentration of residual chloride. Indeed, Yin et al.³¹ also found a beneficial effect of acetone vs. water during NH₃ decomposition over Ru/CNT catalysts. They concluded that water enhances the anchoring of residual chloride on the carbon support during the catalyst preparation. In fact, residual chloride coming from the Ru precursor (RuCl₃) is well known to act as a strong inhibitor of the Ru/C catalysts affecting negatively the catalytic performance. As previously observed, the presence of residual chloride inhibited the adsorption of CO on the Ru surface. Since the CO bond dissociation is the rate-determining step for the methanation reaction, such poor activity in presence of residual chloride was expected.

Table 7. Results of the CSCWG of 10 wt % isopropanol for Ru/C catalysts performed at 450 °C, 30 MPa with $WHSV_{gRu} = 5202 \text{ g}_{Org} \text{ g}_{Ru}^{-1} \text{ h}^{-1}$.

Catalyst	Time [h]	X _c [%]	TOF [s ⁻¹]	GE _c [%]	R _{Coke dep.} [mmol C min ⁻¹]	Gas composition [vol %]					
						CH ₄	CO ₂	H ₂	CO	C ₂ H ₆	C ₃ H _x
0.5% Ru/C _w	6	25	2.4	17	1.2	46.7	16.5	36.2	0.2	< 0.1	< 0.1
	24	10	0.9	3	1.0	3.2	0.6	96.0	0.2	< 0.1	3.7
2% Ru/C _w	6	15	2.6	5	1.4	22.1	9.5	68.1	0.2	< 0.1	2.9
2% Ru/C _a	6	62	4.3	49	2	56.0	22.1	21.6	0.3	< 0.1	< 0.1

The stability of the 0.5% Ru/C_w catalyst was assessed at a high $WHSV_{gRu}$ of 5202 $\text{g}_{Org} \text{ g}_{Ru}^{-1} \text{ h}^{-1}$. After 6 h of CSCWG, the experiment was carried on overnight to reach a total of 24 h on-stream. Surprisingly, the catalyst was completely deactivated with an observed activity close to the one obtained during SCWG performed over the neat carbon support material (compare Table 3). It is also interesting to note the very low GE_c showing that the

carbon contained in the feed could not be converted to the gas phase and most likely remained inside the reactor (as coke). For all the catalysts tested, GE_C was inferior to X_C , confirming that coke formation occurred for all catalysts. Furthermore, their corresponding coke deposition rate has been calculated and their values are in the same range. This supports two parallel reactions: i) coke formation on the support, and ii) catalytic decomposition on the Ru. Some of the coke, likely at the interface of the Ru NPs and the support, may react with H_2 to form some CH_4 . The high H_2 concentration and the low CH_4 concentration for the 0.5% Ru/C_w can both be easily explained by the inhibition of the methanation reaction due to a complete catalyst deactivation. In addition, the presence of C_3H_x indicates that the catalyst is not able to cleave all C-C bonds. As illustrated in Table 8, a considerable loss of the porosity was measured after 24 h of CSCWG for the 0.5% Ru/C_w , whereas the porosity was almost unaffected for the 2% Ru/C_w and the 2% Ru/C_a after 6 h. This is an interesting observation revealing that coke deposition leads to a relatively slow catalyst deactivation. The 2% Ru/C_a was least affected by this deactivation. The high porosity of the 2% Ru/C_a after 96 h was due to the high catalytic activity showing that coke deposition hardly took place. It is important to keep in mind that the amount of catalyst in the reactor was ca. four times higher ($5202 \text{ g}_{Org} \text{ g}_{Ru}^{-1} \text{ h}^{-1}$ instead of $1228 \text{ g}_{Org} \text{ g}_{Ru}^{-1} \text{ h}^{-1}$) meaning that a fraction of the catalytic bed was probably already deactivated and the high porosity measured came from a bed fraction still unaffected by coke deposits. Another interesting phenomenon is shown in Table 8 for the 2% Ru/C_a . While his total pore volume remains nearly constant, the volume of the mesopores decreases while at the same time the one of the micropores increases to twice the value of the fresh support. Because this phenomenon occurs only after a long time, it remained undiscovered in our previous experiments. At this time, we have no good explanation but we assume that the harsh reaction environment with a high partial pressure of H_2 may form additional micropores.

Table 8. Physical structure of the fresh and spent Ru/C catalysts.

Sample	Time [h]	WHSV _{gRu} [g _{Org} g _{Ru} ⁻¹ h ⁻¹]	V _{mesop.} [cm ³ g ⁻¹]	V _{microp.} [cm ³ g ⁻¹]
0.5% Ru/C _w	0	N.A.	0.75	0.13
	24	5202	0.60	0.02
2% Ru/C _w	0	N.A.	0.73	0.11
	6	5202	0.75	0.11
2% Ru/C _a	0	N.A.	0.54	0.11
	6	5202	0.51	0.12
	96	1228	0.41	0.24

The N₂-physisorption results have shown that CSCWG of isopropanol led to a loss of the porosity strengthening the decrease of the catalyst lifetime caused by coke deposits. It was reported by Wambach et al.⁴⁰ that the catalyst deactivation of a commercial 2% Ru/C during CSCWG of aqueous organics was due to a coverage of the Ru NPs by a thin carbonaceous layer. In Figure 9, the Ru NPs coverage by coke seems to be confirmed by the H₂-TPR results of the fresh and spent 0.5% Ru/C_w catalysts. In fact, the H₂ uptake for the reduction of RuO₂ was about four times smaller for the aged catalyst indicating that a considerable fraction of Ru was not available. Concerning the other reduction peaks at higher temperature, almost all disappeared after CSCWG showing that the weakly bonded carbon species and/or the surface functional groups were removed during CSCWG.

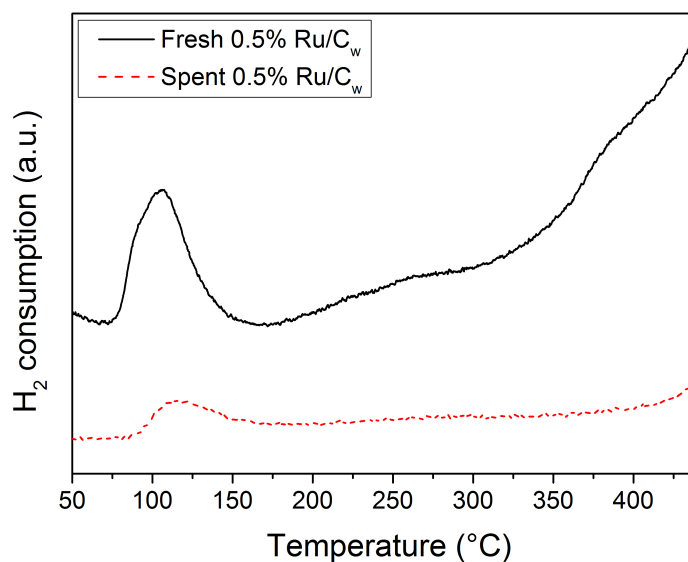


Figure 9. H₂-TPR profiles of the fresh and spent 0.5% Ru/C_w catalysts.

As shown in Figure 10, after 24 h of CSCWG the Ru NPs size of the 0.5% Ru/C_w has slightly increased to a value of 4.9 ± 1.4 nm. By comparing the histogram of the particle size distribution for the fresh and spent 0.5% Ru/C_w (compare Figure 2 (a) and Figure 10), it seems that the distribution slightly shifted to larger particle sizes indicating that small Ru NPs sintered during CSCWG. Such a small Ru NPs growth was already reported by Waldner et al.⁴ and Dreher et al.⁴¹ under similar conditions.

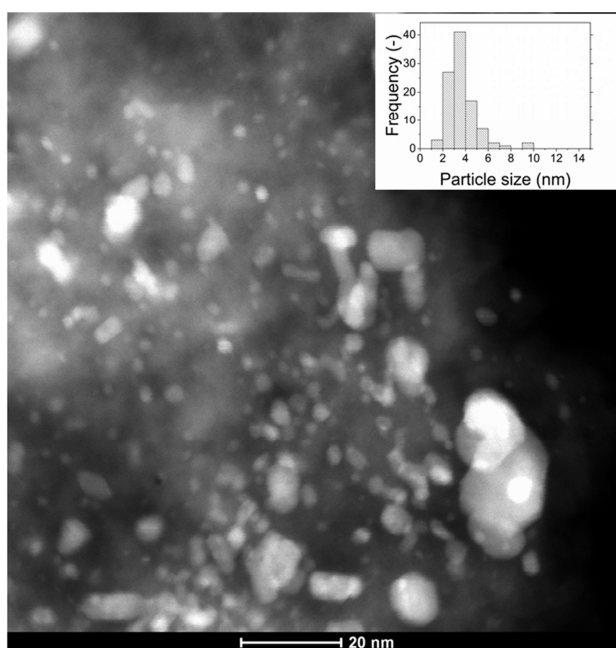


Figure 10. HAADF-STEM image of the spent 0.5% Ru/C_w catalyst.

Conclusions

In this work catalytic supercritical water gasification of isopropanol over Ru/C catalysts was studied. It was shown that isopropanol decomposed to solid carbon (coke), H₂, and water over the neat carbon support in absence of Ru. Although the Ru/C catalysts revealed a high activity as well as a high CH₄ selectivity during CSCWG, the decrease of the catalyst lifetime caused by a progressive coke deposition was the main cause for the complete loss of the catalytic activity. The latter deactivation was due to the decomposition of isopropanol over the carbon surface leading to coke. It was found that a higher Ru dispersion was beneficial for the improvement of the catalytic activity. The use of acetone during the catalyst preparation favored a higher Ru dispersion and reduced significantly the amount of residual chloride coming from the salt precursor (RuCl₃). As a result the TOF was twice higher than for the Ru/C catalyst prepared with water. Since the presence of residual chloride has inhibited the CO adsorption on the Ru surface, the performance of the methanation was significantly

reduced suggesting that the use of a chloride free salt precursor would be required for the improvement of the catalytic performance.

Acknowledgements

This work was financially supported in the frame of the SunCHem project by the Competence Center Energy and Mobility (CCEM-CH) and Swisselectric Research. The authors would like to thank Erich De Boni, and Marian Dreher for the construction of the plug flow reactor setup, Albert Schuler for the ICP-OES analyses, Martin Elsener for the CO pulse chemisorption measurements, Jörg Wambach for the XPS measurements, Xiaoying Xu for the GC-MS measurements, and Alexander Wokaun for the fruitful discussions.

References

1. A. A. Peterson, F. Vogel, R. P. Lachance, M. Froeling, M. J. Antal Jr., and J. W. Tester, *Energy Environ. Sci.*, 2008, **1**, 32–65.
2. D. J. M. De Vlieger, B. L. Mojet, L. Lefferts, and K. Seshan, *J. Catal.*, 2012, **292**, 239–245.
3. F. Vogel, in *Handbook of Green Chemistry*, ed. R. H. Crabtree, Weinheim, WILEY-VCH., 2009, vol. 2, pp. 281–324.
4. M. H. Waldner, F. Krumeich, and F. Vogel, *J. Supercrit. Fluids*, 2007, **43**, 91–105.
5. D. C. Elliott, M. R. Phelps, L. J. Sealock, and E. G. Baker, *Ind. Eng. Chem. Res.*, 1994, **33**, 566–574.
6. X. D. Xu Matsumura, Y., Stenberg, J., Antal, M. J., *Ind. Eng. Chem. Res.*, 1996, **35**, 2522–2530.
7. X. D. Xu and M. J. Antal, *Environ. Prog.*, 1998, **17**, 215–220.
8. I. G. Lee and S. K. Ihm, *Ind. Eng. Chem. Res.*, 2009, **48**, 1435–1442.

9. M. J. Antal, S. G. Allen, D. Schulman, X. D. Xu, and R. J. Divilio, *Ind. Eng. Chem. Res.*, 2000, **39**, 4040–4053.
10. G. W. Huber, J. W. Shabaker, and J. A. Dumesic, *Science (80-.)*, 2003, **300**, 2075–2077.
11. Y. Li, L. Guo, X. Zhang, H. Jin, and Y. Lu, *Int. J. Hydrogen Energy*, 2010, **35**, 3036–3045.
12. R. R. Davda, J. W. Shabaker, G. W. Huber, R. D. Cortright, and J. A. Dumesic, *Appl. Catal. B-Environmental*, 2003, **43**, 13–26.
13. A. Sharma, H. Nakagawa, and K. Miura, *Fuel*, 2006, **85**, 2396–2401.
14. B. Yan, J. Wu, C. Xie, F. He, and C. Wei, *J. Supercrit. Fluids*, 2009, **50**, 155–161.
15. T. Yoshida and Y. Oshima, *Ind. Eng. Chem. Res.*, 2004, **43**, 4097–4104.
16. A. Yamaguchi, N. Hiyoshi, O. Sato, K. K. Bando, M. Osada, and M. Shirai, *Catal. Today*, 2009, **146**, 192–195.
17. K. Pinkwart, T. Bayha, W. Lutter, and M. Krausa, *J. Power Sources*, 2004, **136**, 211–214.
18. A. J. Byrd, S. Kumar, L. Kong, H. Ramsurn, and R. B. Gupta, *Int. J. Hydrogen Energy*, 2011, **36**, 3426–3433.
19. A. J. Byrd, K. K. Pant, and R. B. Gupta, *Fuel*, 2008, **87**, 2956–2960.
20. A. May, J. Salvado, C. Torras, and D. Montane, *Chem. Eng. J.*, 2010, **160**, 751–759.
21. G. van Rossum, B. Potic, S. R. A. Kersten, and W. P. M. van Swaaij, *Catal. Today*, 2009, **145**, 10–18.
22. P. Azadi, J. Otomo, H. Hatano, Y. Oshima, and R. Farnood, *Int. J. Hydrogen Energy*, 2010, **35**, 3406–3414.
23. A. G. Chakinala, S. Kumar, A. Kruse, S. R. A. Kersten, W. P. M. van Swaaij, and D. W. F. Brilman, *J. Supercrit. Fluids*, 2013, **74**, 8–21.
24. M. Dreher, ETH Zurich, Switzerland, 2013.
25. D. J. M. De Vlieger, L. Lefferts, and K. Seshan, *Green Chem.*, 2014, **16**, 864–874.
26. D. C. Elliott, T. R. Hart, and G. G. Neuenschwander, *Ind. Eng. Chem. Res.*, 2006, **45**, 3776–3781.
27. A. Borodzinski and M. Bonarowska, *Langmuir*, 1997, **13**, 5613–5620.
28. Z. Y. Ding, M. A. Frisch, L. X. Li, and E. F. Gloyna, *Ind. Eng. Chem. Res.*, 1996, **35**, 3257–3279.

29. P. Azadi and R. Farnood, *Int. J. Hydrogen Energy*, 2011, **36**, 9529–9541.
30. H. Zoehrer, F. Mayr, and F. Vogel, *Energy Fuels*, 2013, **27**, 4739–4747.
31. S. F. Yin, B. Q. Xu, W. X. Zhu, C. F. Ng, X. P. Zhou, and C. T. Au, *Catal. Today*, 2004, **93-5**, 27–38.
32. M. Cerro-Alarcon, A. Maroto-Valiente, I. Rodriguez-Ramos, and A. Guerrero-Ruiz, *Carbon N. Y.*, 2005, **43**, 2711–2722.
33. Y. Li, C. Pan, W. Han, H. Chai, and H. Liu, *Catal. Today*, 2011, **174**, 97–105.
34. I. Rossetti, N. Pernicone, and L. Forni, *Appl. Catal. a-General*, 2003, **248**, 97–103.
35. A. Guerrero-Ruiz, P. Badenes, and I. Rodriguez-Ramos, *Appl. Catal. a-General*, 1998, **173**, 313–321.
36. Y. C. Chiang, W. H. Lin, and Y. C. Chang, *Appl. Surf. Sci.*, 2011, **257**, 2401–2410.
37. F. Masini, C. E. Strebler, D. N. McCarthy, A. U. F. Nierhoff, J. Kehres, E. M. Fiordaliso, J. H. Nielsen, and I. Chorkendorff, *J. Catal.*, 2013, **308**, 282–290.
38. S. B. Vendelbo, M. Johansson, D. J. Mowbray, M. P. Andersson, F. Abild-Pedersen, J. H. Nielsen, J. K. Norskov, and I. Chorkendorff, *Top. Catal.*, 2010, **53**, 357–364.
39. M. P. Andersson, F. Abild-Pedersen, I. N. Remediakis, T. Bligaard, G. Jones, J. Engbæk, O. Lytken, S. Horch, J. H. Nielsen, and J. Sehested, *J. Catal.*, 2008, **255**, 6–19.
40. J. Wambach, M. Schubert, M. Doebeli, and F. Vogel, *Chimia (Aarau).*, 2012, **66**, 706–711.
41. M. Dreher, B. Johnson, A. A. Peterson, M. Nachtegaal, J. Wambach, and F. Vogel, *J. Catal.*, 2013, **301**, 38–45.